Front. Optoelectron. 2020, 13(4): 409–417
https://doi.org/10.1007/s12200-019-0926-1

RESEARCH ARTICLE

Ripening-resistance of Pd on TiO_2(110) from first-principles kinetics

Qixin WAN[1,2], Hao LIN[3,4], Shuai WANG[1], Jiangnan DAI (✉)[1], Changqing CHEN[1]

1 Wuhan National Laboratory for Optoelectronics, Huazhong University of Science and Technology, Wuhan 430074, China
2 Key Laboratory for Optoelectronics and Communication of Jiangxi Province, Jiangxi Science and Technology Normal University, Nanchang 330013, China
3 State Key Laboratory of Catalysis, Dalian Institute of Chemical Physics, Chinese Academy of Sciences, Dalian 110623, China
4 University of Chinese Academy of Sciences, Chinese Academy of Sciences, Beijing 100049, China

Abstract Suppressing sintering of supported particles is of importance for the study and application of metal-TiO_2 system. Theoretical study of Ostwald ripening of TiO_2(110)-supported Pd particles would be helpful to extend the understanding of the sintering. In this paper, based on density functional theory (DFT), the surface energy of Pd and the total activation energy (the sum of formation energy and diffusion barrier) of TiO_2-supported Pd were calculated. Since the total activation energy is mainly contributed from the formation energy, it is indicated that the ripening of Pd particles would be in the interface control limit. Subsequently, the calculated surface energy and total activation energy were used to simulate Ostwald ripening of TiO_2(110)-supported Pd particles. As a result, in comparison with larger particles, smaller particles would worsen the performance of ripening-resistance according to its lower onset temperature and shorter half-life time. The differences on ripening-resistance among different size particles could be mitigated along with the increase of temperature. Moreover, it is verified that the monodispersity can improve ripening resistance especially for the smaller particles. However, the different performances of the ripening originating from difference of the relative standard deviation are more obvious at higher temperature than lower temperature. This temperature effect for the relative standard deviation is the inverse of that for the initial main particle size. It is indicated that the influence of dispersity of TiO_2(110)-supported Pd particles on ripening may be more sensitive at higher temperature. In this contribution, we extend the first principle kinetics to elaborate the ripening of Pd on TiO_2(110). It is expected that the information from first principle kinetics would be helpful to the study in experiments.

Keywords first-principles, Ostwald ripening, Pd, TiO_2(110)

1 Introduction

The surface properties of metal oxides have attracted great attention for years. Especially, TiO_2 has been studied intensively owing to its wide-ranging applications such as photocatalysis, energy storage, fuel cells and pollution abatement [1–9]. In catalysis, despite the fact that TiO_2 is not itself an efficient catalyst, deposition of metal particles on TiO_2 can significantly enhance the catalytic activity. For more active sites, decreasing the size of metal particles with increasing surface-to-volume ratio which maximizes the surface area exposed to the reactant is the most popular way to design the efficient catalytic system. However, metal atoms in smaller particles with higher chemical potential generally exhibit a larger thermodynamic driving force to sinter or agglomerate and thereby the number of active sites decreases at realistic technology process conditions [10–13]. Thus, suppressing sintering of supported particles becomes one of the dominant issues for gaining efficient catalysts.

As TiO_2(110) is thermally stable, reducible and nonpolar, TiO_2(110) is used as the support in fundamental as well as in industrial research. In metal-TiO_2(110) system, sintering of supported metals is frequently evidenced in experiments [14–16]. Take Pd on TiO_2(110) for example, by studying the sintering of Pd particle after

Received April 24, 2019; accepted June 17, 2019

E-mail: daijiangnan@mail.hust.edu.cn

annealing, researchers suggested that the sintering of Pd particles could be attributed to the particle migration and coalescence [17–19], in which the growth of the particles is by the whole metal particles diffusion across the support surface. However, Howard et al. [20] indicated that the evolution of the size distribution observed in real time by scanning tunnelling microscopy (STM) is consistent with Ostwald ripening mechanism in which larger particles grow at expense of smaller particles through the migration of atoms. Although Su et al. suggested that particle coalescence is possible only for clusters with less than 5 Pd atoms while bigger Pd particles prefer to grow through Ostwald ripening on the $CeO_2(111)$ surface [21], the real system may be more complicated in which two mechanisms are both likely in the process of sintering [22]. Obviously, there is still room for discussion regarding sintering mechanism of $TiO_2(110)$-supported Pd. The process of particle migration and coalescence can be directly observed by the modern technology such as *in situ* transmission electron microscope (TEM). Nevertheless, the process of the migration of atoms of Ostwald ripening is difficult to be captured. Thus, the theoretical study of Ostwald ripening of $TiO_2(110)$-supported Pd particles would be helpful to extend the understanding of the sintering.

Simultaneously, the initial size of particles can largely influence the sintering of the supported particles. Campbell suggested that the metal adsorption energies increase with increasing size of the nanoparticles until their diameter exceeds about 6 nm [23]. It is indicated that the smaller particles could be more unstable than bigger particles. Subsequently, Hu and Li found that the smaller particles have lower onset temperature and shorter half-life time for the ripening of supported particles [24]. Moreover, the sintering of Pd particles is a strong function of the initial conditions such as the initial particle size [24,25]. Recently, it is found that the sintering rates of Al_2O_3-supported Pd particles with a larger initial particle size were slower than those with smaller ones [26]. However, similar size effect has not yet been quantitatively addressed for Pd on $TiO_2(110)$ until now.

During recent years, a kinetic method was developed to study of Ostwald ripening according to an ab initio atomistic thermodynamic theory [27–29]. The Ostwald ripening of late transition metals on $TiO_2(110)$ has been studied by the kinetics [30]. However, the surface energy of the metal is used from the experiments [31]. As we know, many experiments have been successfully discussed by first-principles calculations [32]. Here, based on first-principles calculations including the surface energy and the total activation energy, we will extend the kinetic method of Ostwald ripening to provide quantitative information on $TiO_2(110)$-supported Pd particles. It will be helpful to further improve our understanding of the sintering of $TiO_2(110)$-supported metal particles.

2 Theoretical method

2.1 Ripening kinetics

The generalized kinetics rate equation of Ostwald ripening (OR) for supported particles under reaction condition was formulated in the earlier work (and reference therein) [28,33]. The fundamental rate equation is derived from microscopic origin and can be applied to a wide range of temperature, pressure, composition, support and particle distribution. When one particle with a curvature radius (R) on one support, the ripening rate equation for the supported particle is

$$\frac{\mathrm{d}R}{\mathrm{d}t} = A(R)\left(\exp\left[\frac{\Delta\mu(R'')}{k_{\mathrm{B}}T}\right] - \exp\left[\frac{\Delta\mu(R)}{k_{\mathrm{B}}T}\right]\right)\exp\left[-\frac{E_{\mathrm{tot}}}{k_{\mathrm{B}}T}\right]. \tag{1}$$

Three main parts are included in this equation. There are the prefactor part $A(R)$, chemical potential part $\Delta\mu(R)$ and total activation energy part (E_{tot}). Prefactor $A(R)$ is bound up with the ripening mechanism (diffusion and interface control). It can be largely influenced by the shape and size of supported particles. Detailed description about prefactor $A(R)$ can be found in Ref. [29].The critical curvature radius R'' is the size of particles when the monomer attachment and detachment are in dynamic balance. k_{B} is Boltzmann constant and T is temperature.

Chemical potential of atoms in supported particles with regard to bulk counterpart $\Delta\mu(R)$ is approximated here by Gibbs-Thomson (G-T) relation [34].

$$\Delta\mu(R) = \frac{2\,\Pi\,\gamma}{R}, \tag{2}$$

where Π and γ are the volume of the atom and the surface energy of supported metal particles respectively. When the particle size is small than 6 nm diameter, γ would frequently depend on the size of the supported particles. It originates from that the coordination number of atoms of the surface decreases as the size decreases. Considering modest influence on the result of ripening [35], we ignored the effect of the change of γ with size. For simplicity, the surface energy of Pd particles (88.1 meV/Å^2) originating from the DFT calculation in Section 3.1 was used in the kinetics of ripening.

E_{tot} is the total activation energy of ripening process. It is the sum of the formation energy (E_{f}) of monomer or metal-reactant complexes and corresponding diffusion barrier (E_{d}),

$$E_{\mathrm{tot}} = E_{\mathrm{f}} + E_{\mathrm{d}}, \tag{3}$$

$$E_{\mathrm{f}} = E_{\mathrm{ma/ox}} - E_{\mathrm{ox}} - E_{\mathrm{B}}, \tag{4}$$

where $E_{\mathrm{ma/ox}}$ is the total energy of the adatom on the

support, E_{ox} is the total energy of the support, and E_B is the total energy of the bulk metal. $E_{ma/ox}$, E_{ox}, E_B and E_d can be obtained by density functional theory (DFT). The details of the calculations will be presented in Section 2.2.

2.2 DFT calculations

To get the surface energy of Pd and E_{tot}, DFT calculations were performed using the Vienna Ab initio Simulation Program (VASP [36–38]). Surface energy of Pd facets was calculated using the (1×1) slab model, and Γ-centered *k*-point meshes of $\frac{50}{a} \times \frac{50}{b} \times \frac{50}{c}$ were used for slab calculations. Through a series of comprehensive tests, it was determined that vaccum and slab thicknesses of at least 25 Å separated by a 15 Å vacuum layer were sufficient to ensure necessary convergence. The projector-augmented wave (PAW) method together with Perdew-Burke-Erzernhof (PBE) exchange-correlation functional was used. The kinetic energy cutoff was 400 eV. This system was relaxed by using of conjugate-gradient algorithm until the Hellman-Feynman force [39] on each atom was less than 0.02 eV/Å. The surface energy (γ) is computed using the following expression:

$$\gamma = \frac{1}{2A}(E_S - nE_B), \tag{5}$$

where E_S is the total energy of the slab, E_B is the bulk energy for metal Pd, n is the number of Pd unit cell in the slab, and A is the corresponding surface area of the slab.

We used revised Perdew-Burke-Erzernhof (RPBE) exchange-correlation functional, which is believed better to describe the surface adsorption alleviating the potential over binding [40], to calculate E_{tot}. The kinetic energy cutoff for the plane wave basis set was 400 eV. Here the spin polarization was considered in this paper. The optimized crystal parameters of the rutile TiO_2 bulk are a = 4.661 Å, c = 2.968 Å which are comparable with experimental values of a = 4.593 Å, c = 2.958 Å [41]. A (2×4) surface supercell of rutile TiO_2(110) with a slab of four Ti-O layers that was separated from its periodic images by vacuum space of 15 Å was used. For Pd atom adsorption on the surface, the top two Ti-O layers and the adsorbates were allowed to relax while the other atoms in the bottom layers were fixed in their positions. By using conjugate-gradient algorithm, this system was relaxed until the Hellman-Feynman force [39] on each atom was less than 0.03 eV/Å. The Γ point was used to sample the surface Brillouin zone, as has been done in previous studies involving TiO_2 [27,42]. The climbing image nudged elastic band (CI-NEB) method [43,44] was utilized to locate the transition states for the diffusion of a single Pd atom on the surface. In this study, at least seven images (including the initial and final states) were calculated and vibrational analysis showing a single imaginary mode was used to confirm the transition states optimized. In all DFT calculations, we neglected zero-point energies and entropy corrections in this paper.

3 Results

3.1 DFT calculation

DFT calculations were used to obtain the average surface energy of Pd. We considered various orientations of facet-center cubic Pd including (111), (100), (210), (221), (311) and (322). After the surface energies of Pd surfaces considered were calculated, the result is shown in Table 1. Subsequently, Fig. 1 presents the equilibrium morphology of Pd particle which can be obtained according to the Wulff construction. Table 1 shows the exposed facets, corresponding surface energies and ratio. It is clear that (111), (100), (322) and (221) facets cover 49.73%, 15.99%, 14.26% and 14.12% region exposed, respectively. Furthermore, it is found that the average surface energy of 88.1 meV/Å^2 for Pd particle. The difference between the average surface energy and the surface energy of (111) is less than 6 meV/Å^2. The slight difference is in that (111) covers about 50% of the equilibrium morphology of Pd particle. Our calculated average surface energy is close to the measured surface energy of liquid Pd (94 meV/Å^2) [45].

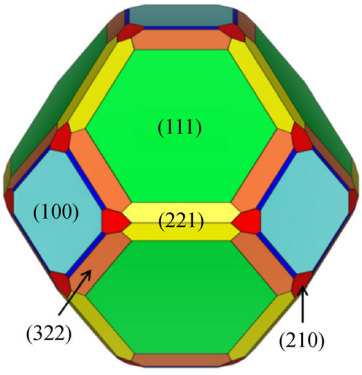

Fig. 1 Equilibrium morphology of faced-centered cubic Pd

Table 1 Calculated surface energies (γ, in meV/Å^2), surface area proportion (f) of the facets exposed on faced-centered cubic (FCC) Pd from Wulff constructions

Pd facets	f_i/%	γ_i/(meV·Å^{-2})
(111)	49.73	82.6
(100)	15.99	95.8
(322)	14.26	90.1
(221)	14.12	91.8
(210)	3.58	101
(311)	2.32	98.8
Σ	100	88.1

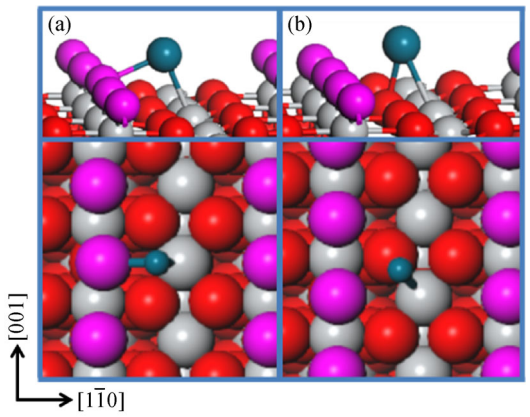

Fig. 2 Side view (top) and top view (bottom) for (a) the most stable atom position and (b) corresponding transition state position of Pd on TiO_2(110). Gray and blue balls represent titanium and palladium atoms. Magenta and red balls represent the upmost bridging oxygens and other oxygens respectively

Subsequently, we calculated the formation energy (E_f) of Pd on TiO_2(110). Various adsorption sites were considered and only the most stable position is indicated below. The most favorable position for Pd on TiO_2(110) is on the hollow site (Fig. 2(a)). Pd atom prefers to bond with a protruded twofold coordinated O atom (O_{2c}) and a fivefold coordinated Ti atom (Ti_{5c}), in line with the previous calculations of Pd [46,47]. Here, the formation energy (E_f) of the most stable position as shown in Fig. 2(a) is 2.05 eV. Transition state (TS) was searched on every possible diffusion path by CI-NEB method. The diffusion barrier (E_d) considered is the least one of the values of the possible diffusion paths. In Fig. 2(b), transition state is on the migration of Pd atom along [001] direction. E_d of Pd along [001] (0.17 eV) is 0.04 eV smaller than the migration along [1$\bar{1}$ 0]. Since E_f is much larger than E_d, it is indicated that the ripening of TiO_2(110)-supported Pd particles are in the interface control limit in which the most of the energy for ripening should be consumed during the detachment/attachment process rather than the diffusion process.

3.2 Ripening of Pd on TiO_2(110)

Firstly, DFT-resulted $\gamma = 88.1$ meV/Å^2 and $E_{tot} = 2.22$ eV were used to investigate the ripening kinetics under temperature programed condition. The initial particle size distribution for Pd particles was set as a normalized Gaussion distribution. For this distribution, the initial main particle size ($\langle d_0 \rangle$) is 3 nm while the relative standard deviation (*rsd*) is 10%. The supported particle ensemble responds to a linear temperature ramp process (temperature programed condition). In the temperature process, the starting temperature is 200 K and subsequent it increases with a rate of 1 K/s. Figure 3 shows the details evolution of TiO_2-supported Pd particles under this temperature programed condition. The evolution of particle size distribution (PSD) is shown in Fig. 3(a). As the ramping temperature is less than 750 K, the change in PSD shape is very slow. When the temperature is at 750 K, it is found that the peak height decreases about 7% and the peak position shifts about 0.1 nm from left to right. When the temperature is higher than 750 K, TiO_2-supported Pd particles ripen faster than before. Moreover, it is obvious that there is a long tail toward the small particles for PSD shape at 850 K in Fig. 3(a). This style of PSD shape is namely Lifshitz-Slyozov-Wagner (LSW)-type distribution. This is because one larger particle needs expense a couple of smaller particles together. In line with above finding in PSD, the normalized dispersion and total particle number plotted in Fig. 3(b) starts to decrease only when the ramping temperature increases up to a threshold. After this, both dispersion and particle number decrease rapidly along with the increase of the average size. Here, onset temperature T_{on}, corresponding 10% decreases of the particle number for ripening under temperature programed

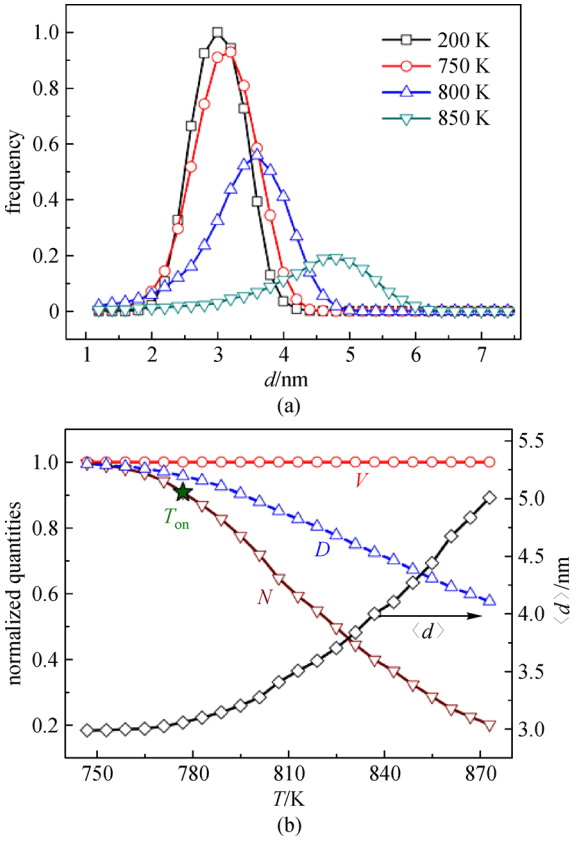

Fig. 3 (a) PSD corresponding to different temperatures; (b) evolution of the normalized volume *V*, dispersion *D* and particle number *N*, and average diameter $\langle d \rangle$ in right *y*-axis versus ramping temperature for Pd on TiO_2(110). Star represents onset temperature T_{on}. The supported particle ensemble responds to a linear temperature ramp process starting from 200 K at a rate of 1 K/s. The contact angle (α) was set as 90°. The surface energy of Pd is 88.1 meV/Å^2. $\langle d_0 \rangle$ = 3 nm, *rsd* = 10%

condition, is defined to compare with experimental results. When $\langle d_0 \rangle$ and *rsd* of TiO_2(110)-supported Pd particles are 3 nm and 10% respectively, resulted T_{on} is 777 K. In comparison with the previous study, the surface energy of Pd used in this paper is lower than that used in the literature [30]. This is understandable that the calculated T_{on} in this paper is about 25 K higher than the previous reported result [30] since particles with lower surface energy would have stronger ripening resistance [29].

To better study the thermal resistance against ripening for Pd on TiO_2(110), OR evolution is performed under isothermal condition. The initial PSD under isothermal condition is the same as those under temperature programed condition. Under isothermal condition (600 K), the evolution of the PSD is shown in Fig. 4(a). First 25% decrease of the particle number of supported Pd particles occurs at t = 5 days. At this time, the peak height decreases about 40% and the peak position right shifts 0.3 nm. When another 25% of the initial particle number decreases, it occurs at t = 14 days and the peak position is at 3.9 nm. While third 25% decrease of the particle number occurs at much late t = 56 days and the corresponding peak at 4.9 nm. At this moment, PSD shape is clearly LSW-type distribution. There is a long tail from 4.9 nm to the smaller size. This PSD shape is similar with that at 850 K under temperature programed condition in Fig. 3(a). It is obvious that the ripening rate gradually decreases with time, accompanying with an increase of the average particle size. In Fig. 4(b), the normalized dispersion and particle number decrease but the average diameter increases with time. It is found that the evolution of Pd dispersion becomes smooth after about 20 days. The variation trend of the Pd particle number is similar to that of Pd dispersion. However, the decreasing rate of Pd particle number is even larger than that of the Pd distribution. Accordingly, the average size increases gradually. To better evaluate the long-time behavior of ripening, the half-life time ($t_{1/2}$), which represents the time necessarily for half decrease of the particle number, is used as measurement of lifetime of Pd particles. When Pd particles ($\langle d_0 \rangle$ = 3 nm and *rsd* = 10%) on TiO_2(110) is at 600 K, resulted $t_{1/2}$ is about 14 days.

Figures 5(a) and 5(b) show the dependence of T_{on} and $t_{1/2}$ on size respectively. It can be found that both T_{on} and $t_{1/2}$ have the linear function with the size of Pd particles. Moreover, both T_{on} and $t_{1/2}$ decrease faster along with the decrease of size. In Fig. 5(a), T_{on} decreases about 300 K with the decrease of $\langle d_0 \rangle$ from 6 to 1 nm. By STM, Howard et al. found Ostwald ripening of TiO_2(110)-supported Pd particles at 750 K. Although the particle diameter in the experiment is from about 3 nm to about 11 nm, the experimental temperature is in our calculated range of T_{on}s. It is found that our calculated T_{on} for particles smaller than 6 nm is lower than the so-called Tamman temperature (914 K, typically half of the bulk melting point of Pd [48]). The origin is that the melting point for smaller particles of Pd is

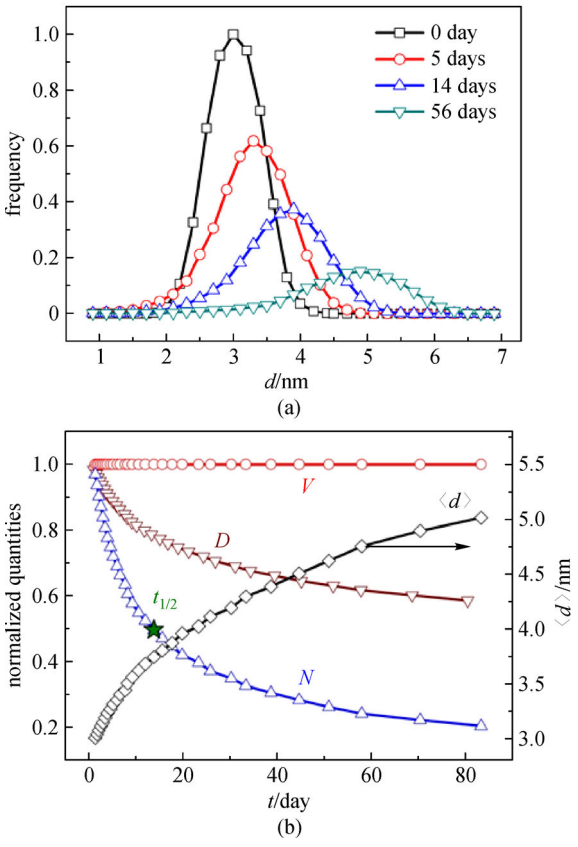

Fig. 4 (a) PSD corresponding to different time; (b) evolution of the normalized volume V, dispersion D and particle number N, and average diameter $\langle d \rangle$ in right y-axis versus ripening time for Pd on TiO_2(110). Star represents half-life time $t_{1/2}$. The contact angle (α) was set as 90°. The surface energy of Pd is 88.1 meV/Å^2. $\langle d_0 \rangle$ = 3 nm, *rsd* = 10%, T = 600 K

smaller than that for the bulk [49]. When the size is higher than 6 nm, the calculated T_{on} could be close to Tamman temperature. Moreover, since Tamman temperature ignores the size and support effect, our calculated results could provide more information to quantitively elaborate the ripening for Pd on TiO_2(110). While $\langle d_0 \rangle$ increases every 1 nm, T_{on} increases more than 45% from 1 to 6 nm but less than 16% from 6 to 16 nm. The increment ratio of T_{on} for increasing every 1 nm is even less than 1% for particles larger than 16 nm. Similar size effect is also found between $t_{1/2}$ and $\langle d_0 \rangle$ as shown in Fig. 5(b). Along with the decrease of $\langle d_0 \rangle$ from 6 to 1 nm, $t_{1/2}$ decreases 5 – 8 orders of magnitude for 300, 450, 600 and 750 K respectively. However, the increment of $t_{1/2}$ for increasing every 1 nm is less than 0.4 orders of magnitude for particles larger than 6 nm. It is concluded the small size would dramatically worsen the resistance against ripening for its lower onset temperature and shorter half-life time. The reason is the smaller particle has higher chemical potential (as indicated in Eq. (2)) to promote ripening. The size effect is more concrete with the small particle size (less than 6 nm). This effect of size dependence on ripening coincides with that

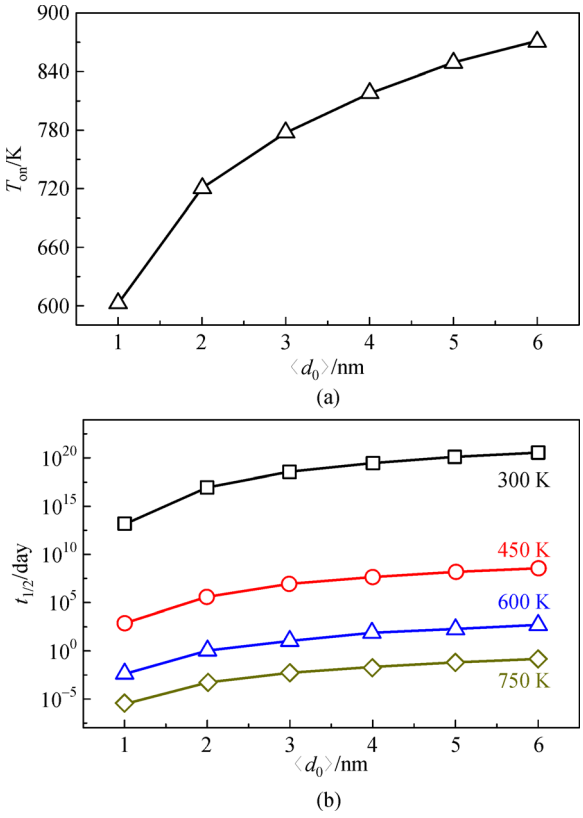

Fig. 5 (a) Onset temperature T_{on} and (b) half-life time $t_{1/2}$ versus different initial average particle diameter $\langle d_0 \rangle$ under the same relative standard deviation rsd = 10%. The contact angle (α) was set as 90°. The surface energy of Pd is 88.1 meV/Å^2

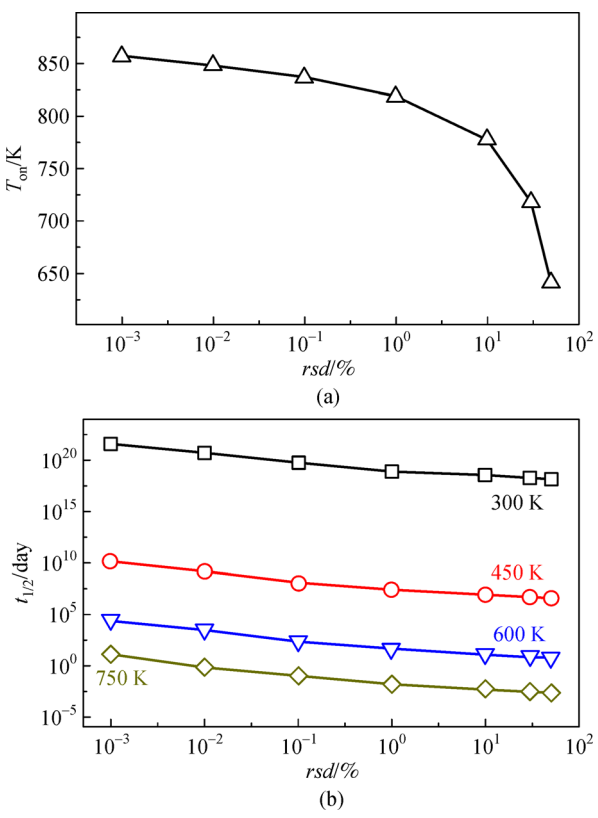

Fig. 6 (a) Onset temperature T_{on} and (b) half-life time $t_{1/2}$ versus relative standard deviation rsd under the same initial $\langle d_0 \rangle$ = 3 nm. The contact angle (α) was set as 90°. The surface energy of Pd is 88.1 meV/Å^2

obtained by Campbell groups [23,50]. To better show the picture of the size effect, Fig. 5 just provides the value of T_{on} and $t_{1/2}$ for particles less than 6 nm. Moreover, along with the increase of temperature from 300 to 750 K, the decrement of $t_{1/2}$ from 1 to 6 nm decreases from about 8 orders of magnitude for 300 K to 5 orders of magnitude for 750 K. It is indicated that higher temperature can mitigate the different performance on ripening originating from the particle size.

Figures 6(a) and 6(b) show the change of T_{on} and $t_{1/2}$ along with rsd. When the monodispersity is the poorest (rsd = 50%), T_{on} and $t_{1/2}$ are 641 K and 6 days (600 K) respectively. On the contrary, when the monodispersity is excellent ($rsd = 10^{-3}$%), T_{on} and $t_{1/2}$ are 857 K and about 2.5×10^4 days (600 K), respectively. It is evident that both T_{on} and $t_{1/2}$ increase along with the size of Pd particles. Furthermore, it is found that T_{on} decreases about 216 K from $rsd = 10^{-3}$% to rsd = 50% while $t_{1/2}$ for $rsd = 10^{-3}$% is about 4166 times of that for rsd = 50%. These results tell us that the monodispersity of TiO_2(110)-supported Pd particles is helpful to mitigate the ripening, particularly for the smaller particles. Simultaneously, $t_{1/2}$ decreases with the increase of temperature. The increment of $t_{1/2}$s for 300 and 450 K, 450 and 600 K as well as 600 and 750 K are about 11, 6 and 4 orders respectively. It is found that the increment of $t_{1/2}$ between every 150 K could decrease along with the increase of the temperature. The difference of $t_{1/2}$ between the poorest monodispersity (rsd = 50%) and the highest monodispersity considered ($rsd = 10^{-3}$%) are about 3.4, 3.5, 3.6 and 3.7 orders of magnitude for 300, 450, 600 to 750 K respectively. The different performance of the ripening originating from different rsds is more obvious at higher temperature than lower temperature. This temperature effect for rsds is the inverse of that for $\langle d_0 \rangle$. It is indicated that the influence of rsd on ripening may be more sensitive at higher temperature.

4 Conclusions

We calculated the surface energy of some exposed facets of face-centered cubic Pd. It is found that (111) covers most of the exposed area of Wulff construction of Pd. The average surface energy of the equilibrium morphology is close to the surface energy of (111). The most stable adsorption of Pd on TiO_2(110) is found that Pd prefers to occupy hollow site. Moreover, it diffuses easier along with [001] than with [$1\bar{1}$ 0] for its lower diffusion barrier.

Subsequently, according to the average surface energy of Pd and the total activation energy (the formation energy and diffusion barrier) calculated from the density functional theory, the ripening of TiO_2(110)-supported Pd particles is simulated by a kinetic method. The result concluded that smaller Pd particles would worsen the performance of ripening-resistance according to its lower onset temperature and shorter half-life time. This size effect could be mitigated along with the increase of temperature. Furthermore, it is verified that the monodispersity can improve ripening resistance especially for the smaller Pd particles. However, the different performance of the ripening originating from difference of the relative standard deviation is more obvious at higher temperature than lower temperature. This temperature effect for the relative standard deviation is the inverse of that for the initial main particle size. It is indicated that the influence of dispersity of TiO_2(110)-supported Pd particles on ripening may be more sensitive at higher temperature. In this contribution, we extend the first principle kinetics to elaborate the ripening of Pd on TiO_2(110). It is expected that the information would be helpful to the study on sintering for metals on oxide in experiments.

Acknowledgements This work was supported by Key Project of Chinese National Development Programs (No. 2018YFB0406602), the National Natural Science Foundation of China (Grant No. 61774065). We thank Prof. W.-X. Li for fruitful discussions and S. Hu for the help of the ripening kinetics.

References

1. Diebold U. The surface science of titanium dioxide. Surface Science Reports, 2003, 48(5–8): 53–229
2. Chen M S, Goodman D W. The structure of catalytically active gold on titania. Science, 2004, 306(5694): 252–255
3. Valden M, Lai X, Goodman D W. Onset of catalytic activity of gold clusters on titania with the appearance of nonmetallic properties. Science, 1998, 281(5383): 1647–1650
4. Fu Q, Wagner T. Interaction of nanostructured metal overlayers with oxide surfaces. Surface Science Reports, 2007, 62(11): 431–498
5. Diebold U, Pan J-M, Madey T E. Ultrathin metal film growth on TiO_2(110): an overview. Surface Science, 1995, 331–333(Part B): 845–854
6. Hu M, Noda S, Komiyama H. A new insight into the growth mode of metals on TiO_2(110). Surface Science, 2002, 513(3): 530–538
7. Persaud R, Madey T E. Chapter 11 Growth, structure and reactivity of ultrathin metal films on TiO_2 surfaces. In: King D A, Woodruff D P, eds. Growth and Properties of Ultrathin Epitaxial Layers. The Chemical Physics of Solid Surfaces, 1997, 8: 407–447
8. Park J B, Ratliff J S, Ma S, Chen D A. *In situ* scanning tunneling microscopy studies of bimetallic cluster growth: Pt–Rh on TiO_2(110). Surface Science, 2006, 600(14): 2913–2923
9. Lei Y, Liu H, Xiao W. First principles study of the size effect of TiO_2 anatase nanoparticles in dye-sensitized solar cell. Modelling and Simulation in Materials Science and Engineering, 2010, 18(2): 025004
10. Bartholomew C H. Mechanisms of catalyst deactivation. Applied Catalysis A, General, 2001, 212(1–2): 17–60
11. Moulijn J A, van Diepen A E, Kapteijn F. Catalyst deactivation: is it predictable? what to do? Applied Catalysis A, General, 2001, 212 (1–2): 3–16
12. Forzatti P, Lietti L. Catalyst deactivation. Catalysis Today, 1999, 52 (2-3): 165–181
13. McCarty J G, Gusman M, Lowe D M, Hildenbrand D L, Lau K N. Stability of supported metal and supported metal oxide combustion catalysts. Catalysis Today, 1999, 47(1-4): 5–17
14. Bugyi L, Óvári L, Kónya Z. The formation and stability of Rh nanostructures on TiO_2(110) surface and TiO_x encapsulation layers. Applied Surface Science, 2013, 280: 60–66
15. Piwoński I, Spilarewicz-Stanek K, Kisielewska A, Kądzioła K, Cichomski M, Ginter J. Examination of Ostwald ripening in the photocatalytic growth of silver nanoparticles on titanium dioxide coatings. Applied Surface Science, 2016, 373: 38–44
16. Madej E, Spiridis N, Socha R P, Wolanin B, Korecki J. The nucleation, growth and thermal stability of iron clusters on a TiO_2(110) surface. Applied Surface Science, 2017, 416: 144–151
17. Jak M J J, Konstapel C, van Kreuningen A, Verhoeven J, Frenken J W M. Scanning tunnelling microscopy study of the growth of small palladium particles on TiO_2(110). Surface Science, 2000, 457(3): 295–310
18. Stone P, Bennett R A, Poulston S, Bowker M. Scanning tunnelling microscopy and Auger electron spectroscopy study of Pd on TiO_2(110). Surface Science, 1999, 433–435(2): 501–505
19. Stone P, Poulston S, Bennett R A, Bowker M. Scanning tunnelling microscopy investigation of sintering in a model supported catalyst: nanoscale Pd on TiO_2(110). Chemical Communications, 1998, 13: 1369–1370
20. Howard A, Mitchell C E J, Egdell R G. Real time STM observation of Ostwald ripening of Pd nanoparticles on TiO_2(110) at elevated temperature. Surface Science, 2002, 515(2 – 3): L504–L508
21. Su Y Q, Liu J X, Filot I A W, Hensen E J M. Theoretical study of ripening mechanisms of Pd clusters on ceria. Chemistry of Materials, 2017, 29(21): 9456–9462
22. Hansen T W, Delariva A T, Challa S R, Datye A K. Sintering of catalytic nanoparticles: particle migration or Ostwald ripening? Accounts of Chemical Research, 2013, 46(8): 1720–1730
23. Campbell C T. The energetics of supported metal nanoparticles: relationships to sintering rates and catalytic activity. Accounts of Chemical Research, 2013, 46(8): 1712–1719
24. Hu S, Li W X. Influence of particle size distribution on lifetime and thermal stability of Ostwald ripening of supported particles. ChemCatChem, 2018, 10(13): 2900–2907
25. Wynblatt P, Gjostein N A. Supported metal crystallites. Progress in Solid State Chemistry, 1975, 9: 21–58
26. Kang S B, Lim J B, Jo D, Nam I S, Cho B K, Hong S B, Kim C H, Oh S H. Ostwald-ripening sintering kinetics of Pd-based three-way catalyst: importance of initial particle size of Pd. Chemical Engineering Journal, 2017, 316: 631–644
27. Goldsmith B R, Sanderson E D, Ouyang R, Li W X. CO- and NO-induced disintegration and redispersion of three-way catalysts rhodium, palladium, and platinum: an ab initio thermodynamics

study. Journal of Physical Chemistry C, 2014, 118(18): 9588–9597
28. Ouyang R, Liu J X, Li W X. Atomistic theory of Ostwald ripening and disintegration of supported metal particles under reaction conditions. Journal of the American Chemical Society, 2013, 135 (5): 1760–1771
29. Hu S, Li W X. Theoretical investigation of metal-support interactions on ripening kinetics of supported particles. ChemNanoMat: Chemistry of Nanomaterials for Energy, Biology and More, 2018, 4(5): 510–517
30. Wan Q, Hu S, Dai J, Chen C, Li W X. First-principles kinetic study for Ostwald ripening of late transition metals on TiO_2(110). Journal of Physical Chemistry C, 2019, 123(2): 1160–1169
31. Vitos L, Ruban A V, Skriver H L, Kollár J. The surface energy of metals. Surface Science, 1998, 411(1 – 2): 186–202
32. Zhao C, Wan Q, Dai J, Zhang J, Wu F, Wang S, Long H, Chen J, Chen C, Chen C. Diluted magnetic characteristics of Ni-doped AlN films via ion implantation. Frontiers of Optoelectronics, 2017, 10 (4): 363–369
33. Parker S C, Campbell C T. Kinetic model for sintering of supported metal particles with improved size-dependent energetics and applications to Au on TiO_2(110). Physical Review B, 2007, 75(3): 035430
34. Johnson C A. Generalization of the Gibbs-Thomson equation. Surface Science, 1965, 3(5): 429–444
35. Parker S C, Campbell C T. Reactivity and sintering kinetics of Au/TiO_2(110) model catalysts: particle size effects. Topics in Catalysis, 2007, 44(1–2): 3–13
36. Kresse G, Furthmüller J. Efficient iterative schemes for ab initio total-energy calculations using a plane-wave basis set. Physical Review B, 1996, 54(16): 11169–11186
37. Kresse G, Furthmüller J. Efficiency of ab-initio total energy calculations for metals and semiconductors using a plane-wave basis set. Computational Materials Science, 1996, 6(1): 15–50
38. Kresse G, Hafner J. Ab initio molecular dynamics for liquid metals. Physical Review B, 1993, 47(1): 558–561
39. Feynman R P. Forces in molecules. Physical Review, 1939, 56(4): 340–343
40. Hammer B, Hansen L B, Nørskov J K. Improved adsorption energetics within density-functional theory using revised Perdew-Burke-Ernzerhof functionals. Physical Review B, 1999, 59(11): 7413–7421
41. Grant F A. Properties of rutile (titanium dioxide). Reviews of Modern Physics, 1959, 31(3): 646–674
42. Kim H Y, Lee H M, Pala R G S, Shapovalov V, Metiu H. CO oxidation by rutile TiO_2(110) doped with V, W, Cr, Mo, and Mn. Journal of Physical Chemistry C, 2008, 112(32): 12398–12408
43. Henkelman G, Jónsson H. Improved tangent estimate in the nudged elastic band method for finding minimum energy paths and saddle points. Journal of Chemical Physics, 2000, 113(22): 9978–9985
44. Henkelman G, Uberuaga B P, Jónsson H. A climbing image nudged elastic band method for finding saddle points and minimum energy paths. Journal of Chemical Physics, 2000, 113(22): 9901–9904
45. Overbury S H, Bertrand P A, Somorjai G A. Surface composition of binary systems. Prediction of surface phase diagrams of solid solutions. Chemical Reviews, 1975, 75(5): 547–560
46. Zhao W, Lin H, Li Y, Zhang Y, Huang X, Chen W. Growth mechanism of palladium clusters on rutile TiO_2(110) surface. Journal of Natural Gas Chemistry, 2012, 21(5): 544–555
47. Sanz J F, Márquez A. Adsorption of Pd atoms and dimers on the TiO_2(110) surface: a first principles study. Journal of Physical Chemistry C, 2007, 111(10): 3949–3955
48. Kittel C. Introduction to Solid State Physics. New York: John Wiley & Sons, 1966
49. Lu H M, Li P Y, Cao Z H, Meng X K. Size-, shape-, and dimensionality-dependent melting temperatures of nanocrystals. Journal of Physical Chemistry C, 2009, 113(18): 7598–7602
50. Campbell C T, Parker S C, Starr D E. The effect of size-dependent nanoparticle energetics on catalyst sintering. Science, 2002, 298 (5594): 811–814

Qixin Wan received the B.E. degree from Nanchang University in 2004. He is currently pursuing the Ph.D. degree at Huazhong University of Science and Technology. His current research interest is nanomaterials and photoelectric materials.

Hao Lin received the B.E. degree from Wuhan University in 2014. He is currently pursuing the Ph.D. degree at Dalian Institute of Chemical Physics, CAS. His current research interest is crystal phase effects by first principles.

Shuai Wang received the B.E. degree from Huazhong University of Science and Technology in 2013. He is currently pursuing the Ph.D. degree at Huazhong University of Science and Technology. His current research interest is photoelectric device.

Jiangnan Dai received the B.E. degree from Hunan University of Science and Technology in 2002, and the Ph.D. degree from Nanchang University in 2007. Since 2010, he has been an associate professor at Huazhong University of Science and Technology, where he worked on photoelectric device based on wide bandgap semiconductor.

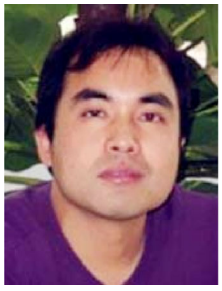

Changqing Chen received the B.E. degree from Wuhan University in 1992, and the Ph.D. degree from University of Erlangen-Nürnberg in 2000. Since 2007, he has been a professor at Huazhong University of Science and Technology, where he worked on lighting emitting diode.